

Theory of plasmon-enhanced high-harmonic generation in the vicinity of metal nanostructures in noble gases

A. Husakou,* S.-J. Im, and J. Herrmann

Max Born Institute of Nonlinear Optics and Short Pulse Spectroscopy, Max Born Str 2a, D-12489 Berlin, Germany

(Dated: November 5, 2018)

We present a semiclassical model for plasmon-enhanced high-harmonic generation (HHG) in the vicinity of metal nanostructures. We show that both the inhomogeneity of the enhanced local fields and electron absorption by the metal surface play an important role in the HHG process and lead to the generation of even harmonics and to a significantly increased cutoff. For the examples of silver-coated nanocones and bowtie antennas we predict that the required intensity reduces by up to three orders of magnitudes and the HHG cutoff increases by more than a factor of two. The study of the enhanced high-harmonic generation is connected with a finite-element simulation of the electric field enhancement due to the excitation of the plasmonic modes.

PACS numbers: 42.65.Ky, 78.67.Bf

Progress of contemporary ultrafast laser physics has led to the generation of attosecond laser pulses by high-harmonic generation (HHG) [1] opening the way to exciting opportunities to study time-resolved fundamental electronic processes in atoms and molecules, and to investigate the collective and correlated dynamics of many-electron systems on the attosecond scale [2–8]. On the other hand, in an another rapidly evolving field metallic nanostructures can be used to achieve localization of light on sub-wavelength nanometer scale and to realize huge plasmonic field enhancements in the vicinity of these objects. At present plasmonics has been the subject of extensive theoretical and experimental research and experiences a dramatic growth of applications [9–12]. Recently an interesting experiment has been reported based on a connection of both fields: high-order harmonic generation (HHG) has been demonstrated by nJ pulses directly from a laser oscillator by exploiting the local field enhancement near a metallic bowtie-shaped gold nanoelement [13]. The elimination of complex and expensive amplifiers and the opportunity to perform HHG and attosecond experiments at MHz repetition rates can significantly extend the ability of extreme VUV generation and attosecond pump-probe spectroscopy and will lead to novel applications in lithography and imaging. However, a theoretical description of plasmon-enhanced HHG, which is a key for further progress in this field, is currently missing.

In this paper we present a theoretical investigation of plasmon-enhanced HHG in a noble gas in the vicinity of a silver nanocone and a silver bowtie structure. Our goal is directed to an understanding of the role of metal nanostructures and the inhomogeneous plasmonic field enhancement in the HHG process. We describe the microscopic laser-atom interaction by the time-dependent dipole moment in the semi-classical approximation [14]. In the vicinity of the metal nanostructures the input laser intensity is enhanced by up to three orders of magnitude by the plasmons in so-called "hot spots" and sensitively

depends on the position. This strongly enhanced field ionizes the noble gas atoms, the resulting electrons are accelerated in the enhanced field and recollide with the parent ion, transforming their kinetic energy into high harmonic radiation. In the hot spot, electron experience the inhomogeneous electric field, and some of them will hit the metal surface and never return to the parent ion. We show that both field inhomogeneity and the electron absorption at the metal surface lead to the emission of even harmonics as well as to more than a twofold increase of the cut-off frequency.

We describe HHG in the framework of a model that is an extension of the Lewenstein model modified to account for the field inhomogeneity in the vicinity of the nanostructure, as well as for the electron absorption by the metallic surface. Under the action of the electric field $E(t)$, the electron leaves the atom at the time moment t_s and later recombines with the parent ion at the time t_f . The maximum HHG contribution is provided by electrons with the canonical momentum p for which their position at t_f coincides with that of the parent ion. Neglecting the Coulomb potential and using the stationary phase method [14], the time-dependent high-harmonic dipole moment is given by

$$\begin{aligned} x(t_f) &= i \frac{e}{2\omega_0^{5/2} m_e} \int_{-\infty}^{t_f} \left(\frac{\pi}{\epsilon + i\Delta t/2} \right)^{3/2} H(t_f, t_s) \\ &\times d_x(p(t_s) - eA(t_s)) d_x^*(p(t_f) - eA(t_f)) \\ &\times E(t_f) \exp(-i \frac{S(t_f, t_s)}{\hbar}) dt_s + c.c. \end{aligned} \quad (1)$$

Here ϵ is an arbitrary small parameter, ω_0 is the central frequency, $d_x(p) = i2^{7.25} [\hbar\omega_0 m_e^2 I_p]^{5/4} \pi^{-1} p / (p^2 + \alpha)^3$ with $\alpha = 2m_e^{1/2} I_p^{1/2}$ is the dimensionless dipole matrix element, and $S(t_f, t_s) = \int_{t_s}^{t_f} (I_p + (p(t) - eA(t))^2 / 2m_e) dt$ is the classical action equal in the Lewenstein model to $S_0(t_f, t_s) = I_p \Delta t - 0.5e^2 (\Delta B^2 / \Delta t + \Delta C) / m_e$. Here $\dot{A} \equiv dA(t)/dt = E(t)$, $\dot{B}(t) = A(t)$, $\dot{C}(t) = A^2(t)$, for any function F we define $\Delta F \equiv F(t_f) - F(t_s)$, $\Delta t = t_f - t_s$,

and I_p is the ionization potential. For the unmodified Lewenstein model, in the stationary-phase approximation the canonical momentum is given by $e\Delta B/\Delta t$. $H(t_f, t_s)$ is a function describing the electron absorption at the metal surface; in the unmodified Lewenstein model we have $H(t_f, t_s) \equiv 1$. We extend the semiclassical HHG model accounting for the inhomogeneity of the field in the hot spot by adding the first-derivative term to the field $E(t, x) = E(t)(1 + x/d_{inh})$, and consider this derivative term as a perturbation, including only the first-order correction to the electron trajectory. As a result, the expressions for the momentum $p(t_s)$ and $S(t_f, t_s)$ are modified as follows:

$$p(t_s) = e[A(t_s) + \frac{\Delta B - A(t_s)\Delta t + \beta(0.5(\Delta B)^2 - \Delta D + C(t_s)\Delta t)}{\Delta t - \beta(2\Delta G + \Delta t[B(t) + B(t_s)])}], \quad (2)$$

$$S(t_f, t_s) = S_0(t_f, t_s) + e^2\beta m_e^{-1} \{p(t_s)^2[2\Delta G + (B(t_f) + B(t_s))\Delta t] + p(t_s)[- \Delta C\Delta t + 2\Delta D] + (C(t_f) + C(t_s))\Delta B - 2\Delta F\}, \quad (3)$$

where $\dot{D}(t) = C(t)$, $\dot{F}(t) = C(t)E(t)$, $\dot{G}(t) = B(t)$, $\beta = e/(m_e d_{inh})$, and T_0 is the optical period. Another modification of the model is described by the function $H(t, t_s)$ under the integral in Eq. (1). This function is equal to 1 unless the electron during the motion hits the metal surface positioned at d_{sur} , otherwise we assume that the electron is absorbed by the surface and set $H(t, t_s) = 0$. We have used the finite-element Maxwell solver JCMwave to model the plasmonic field enhancement in the vicinity of the nanostructure, taking the experimental complex-valued dielectric function of silver. For short input pulses, to include the dispersion of silver and of the field distribution near the nanostructure, we calculated the field distribution for a set of wavelengths within the input pulse spectrum and then reconstructed the position-dependent pulse profile from the wavelength- and position-dependent field. In this paper, we disregard the modification of the field induced by the neighboring structure, the depolarization effects are weak in our case. To prove that the mesh size is small enough, we halved it and found no significant change in the results.

First we analyze the principal effects described by the above extended model in dependence on the model parameters d_{inh} and d_{sur} . To understand the effect of the inhomogeneity of the field and of the metal surface on the HHG process, in Fig. 1 we consider the HHG spectra for different parameters d_{inh} [Fig. 1(a)] and d_{sur} [Fig. 1(b)] for cw radiation with a typical intensity in the hot spot of 200 TW/cm². In Fig. 1(a) even for a very low inhomogeneity, characterized by $d_{inh} = 1000$ nm, the inverse spatial symmetry is broken, which leads to a qualitatively new effect: the generation of even harmonics (shown by the blue crosses). For larger inhomogeneities

with $d_{inh} = 20$ nm the amplitude of the even harmonics approaches that of odd harmonics. Simultaneously, the harmonic cutoff shifts to higher harmonic numbers and become much less pronounced. Due to inhomogeneity, electrons have higher velocities when they reach the parent ion, leading to a higher kinetic energy and therefore to a higher cut-off frequency. The influence of the metal surface and the associated electron absorption is studied in Fig. 1(b). One can see that for a distance to the surface $d_{sur} = 3$ nm, no electron reaches the surface, and correspondingly no modification in the dipole moment and no even harmonics appear. For shorter d_{sur} , some electrons will reach the surface. Since the function $H(t, t_s)$ introduces a sharp modulation in the temporal profile of the harmonics, an extension of the spectrum to higher harmonic numbers can be seen in Fig. 1(b), combined with the emission of even harmonics. From Fig. 1 one can see that the combined effect of the field inhomogeneity

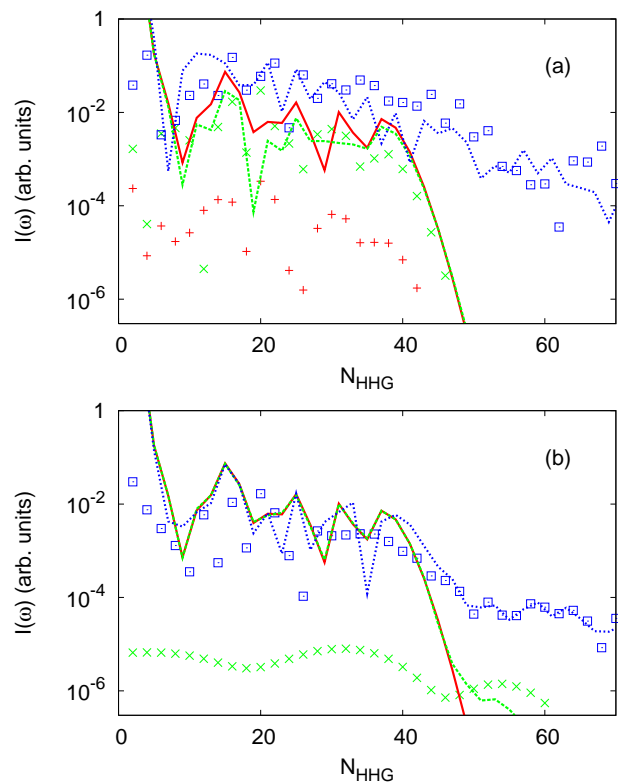


FIG. 1: Influence of the field inhomogeneity (a) and of the metal surface (b) on the HHG process. Odd harmonics are presented by curves while even harmonics are shown by points. In (a), the field has the inhomogeneity scale d_{inh} of 1000 nm (red solid curve and red vertical crosses), 20 nm (green short-dashed curve and green diagonal crosses), and 5 nm (blue long-dashed curve and blue squares). In (b), the distance to the metallic surface d_{sur} is 3 nm (red solid curve), 2.62 nm (green short-dashed curve and green diagonal crosses), and 1.5 nm (blue long-dashed curve and blue squares). For both cases, cw radiation at 830 nm with intensity in the hot spot of 200 TW/cm² in argon is considered.

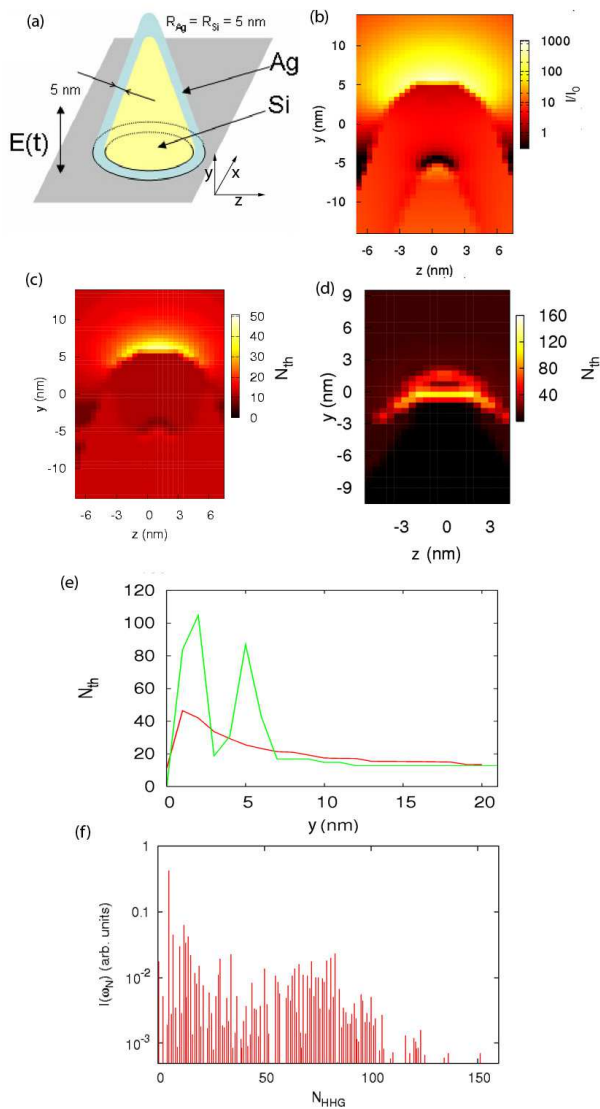


FIG. 2: High harmonic generation in the vicinity of a nanocone structure. In (a), the scheme of the nanocone is shown. The curvature radii and the thickness of silver coating are 5 nm, the y -polarized field propagates along the x direction. In (b) the intensity enhancement is presented for the zy cross-section of the incident field at 830 nm. In (c) and (d), the distribution of the harmonic cutoff is shown for the model without (c) and with (d) modifications by the field inhomogeneity and metal surface for 10-fs input pulses with 0.3 TW/cm^2 intensity and argon surrounding the tip. In (e) the cutoff for the modified (green curve) and unmodified (red curve) model is shown along the y axis, and in (e) the spectrum for cw excitation with the above parameters is shown.

geneity and of the metal surface can increase the HHG cutoff by a factor larger than two.

Next we perform a realistic simulation of HHG in the vicinity of a silver nanocone as depicted in Fig. 2(a). Such nanocone structure can be produced by silver deposition on a chemically created silicon needle without the need of nanoscale lithographic control. The curva-

ture radius of the nanostructure edges is the key parameter determining the maximum field enhancement, with optimum structure having the smallest curvature radius. We have assumed radii of 5 nm, in correspondence with the current state of the manufacturing technique. The spatial field distribution shown in Fig. 2(b) with parameters given in the caption demonstrates intensity enhancement factors of up to 1000 in the "hot spot" in the vicinity of the tip. From the comparison of xy and zy cross-sections (not shown) one can see that the field enhancement is higher on the surface directed towards the incoming beam, but this is a minor effect compared to the strong enhancement near the tip. Note that the field is inhomogeneous on the scale below 10 nm in the "hot spot" which is located directly above the metal surface. The parameters $d_{inh}(x, y, z)$ and $d_{sur}(x, y, z)$ are calculated from this spatial distribution of the field and are used for the HHG simulation by using the extended model as given by Eq. (1)-(3). In Fig. 2(c) and (d) we present the spatial distribution of the harmonic cutoff N_{th} for an excitation by 830-nm sech-shaped pump pulses with intensity of only 0.3 TW/cm^2 , FWHM of 10 fs, and polarization and wavevector as indicated in Fig. 2(a). The field enhancement in the "hot spot" increases the intensity to roughly 300 TW/cm^2 , which for the chosen wavelength corresponds in the unmodified Lewenstein-model to a cut-off of roughly the 50^{th} harmonic, as can be seen in Fig. 2(c). However, due to the effect of the field inhomogeneity and the presence of the metal surface, the cutoff increases up to 105, which correspond to the emission of 150-eV photons using an input intensity of only 0.3 TW/cm^2 . Such pulses can be obtained from a typical laser oscillator without amplifier. In Fig. 2(e) a comparison between the extended model including the effects of the field inhomogeneity and metal surface, and the unmodified Lewenstein model is drawn. The cut-off harmonic number as a function of the position reaches values of above 100 for the modified model, while the unmodified only predicts values around 40. Further from the tip of the nanocone, the field become relatively homogeneous, and the distance to the metal surface is large, therefore both models coincide. Note however, that although the modifications of the Lewenstein model are important only in a small fraction of the volume, it is exactly this volume ("hot spot") which dominate the generation of high harmonics and therefore these modifications become especially important. This is clearly visible in Fig. 2(f), where we show the spectrum of the high harmonics emitted in the x direction integrated over the nanostructure position, where a significant emission of even harmonics as well as the extended and smoothed cutoff can be seen. We have also calculated the phases of the HHG harmonics separately for short and long electron trajectories, and found that the modification of phases due to the field inhomogeneity is negligible for short trajectories but reaches $\pi/2$ for the

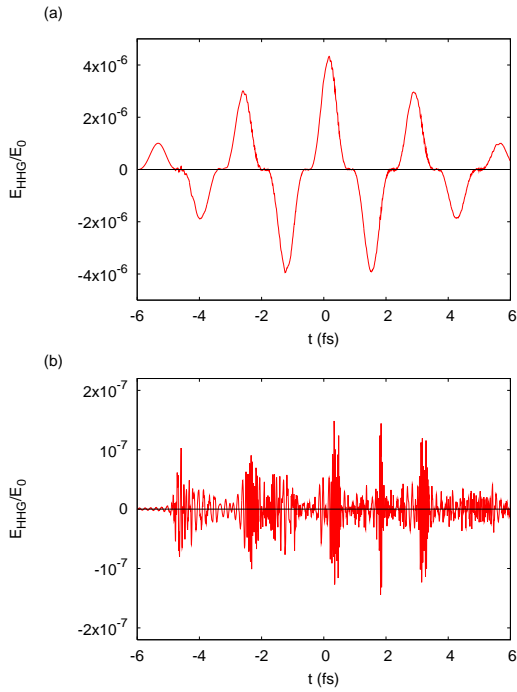


FIG. 3: Temporal shape (a) and the temporal shape after filtering out low harmonics ($N < 40$) of the output(b) with input intensity of 0.3 TW/cm^2 and duration of 10-fs at 830 nm for a nanocone structure.

long ones. This, however, will not influence the divergence of the HHG radiation, since the hot spot is smaller than the typically considered wavelength and is a point-like source. In [15] we calculated the variation of the high-harmonic phases with different intensities depending on the transverse positions in the beam. It is shown that in the considered example the phases change only slightly for different intensities within the beam for harmonic numbers below 50, which can be compensated by an appropriate curvature of the pump beam. For higher harmonic numbers the phases show strong changes, resulting in beam distortion due to irregular spatial modulation.

In Fig. 3, the temporal profile of the output harmonic radiation is shown for 10-fs input pulses. The temporal profile in Fig. 3(a) is dominated by low-order (< 10) harmonics. It is well-known that filtering out the lower harmonics leaves only few electron trajectories with maximum kinetic energy at the recollision time, which can lead to the formation of attosecond pulses. In Fig. 3(b) we present the temporal profile for the above case but with harmonics below the 50th order filtered out. One can see the formation of few pulses with down to 150-attosecond FWHM. These pulses are shorter and more irregular than those obtained from the unmodified model (not shown).

In order to compare the results of our model with experimental measurements, we have simulated high har-

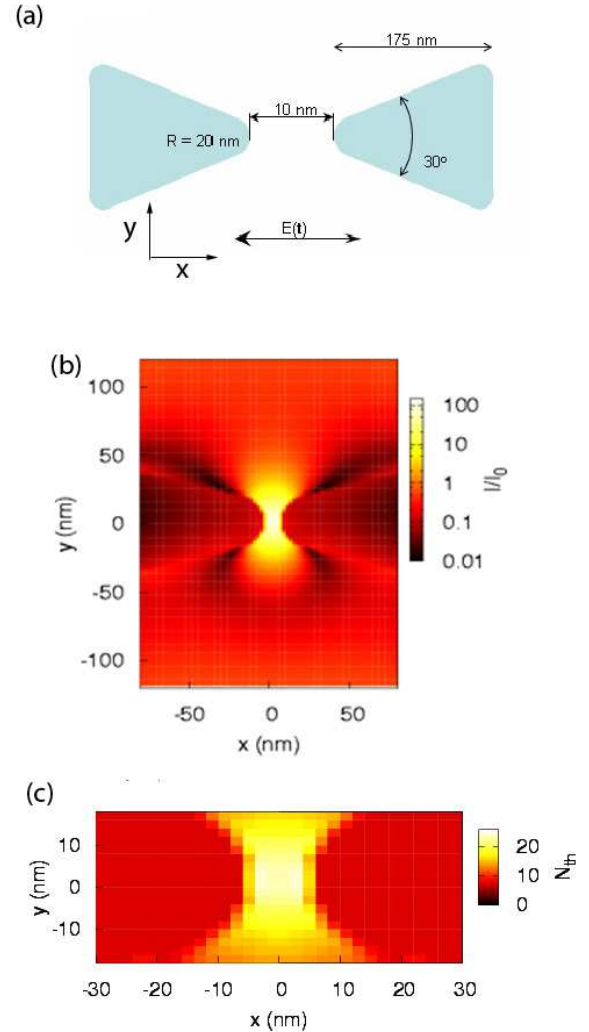


FIG. 4: High harmonic generation in the vicinity of a bowtie structure. In (a), the scheme of the bowtie structure and its geometric parameters are shown, the x -polarized field propagates along y direction. In (b) the field enhancement is presented for the xy cross-section of the incident field at 830 nm; in (c), the distribution of the harmonic cutoff is shown for 10-fs input pulses with 0.5 TW/cm^2 intensity for HHG in argon surrounding the bowtie structure.

monic generation in the vicinity of a bowtie nanoantenna, such as used in Ref. [13]. Structure and parameters of the studied bowtie antennas is shown in Fig. 4(a) consisting of two silver isosceles triangles with curvature radius and distance between the vertices in the range of 10 nm. In Fig. 4(b), the field enhancement by the bowtie antenna with parameters as given in the figure is presented, which shows a "hot spot" between the inner vertices of the triangles and a maximum enhancement of about 10^2 . For other geometrical parameters of the structure, the enhancements drops with increasing curvature radius and distance between the triangle tips. By using this field

enhancement HHG is calculated by using the extended model. In Fig. 4(c) for incident 10-fs pulses with intensity of 0.5 TW/cm^2 the spatial distribution of the threshold harmonic number N_{th} is presented. The calculated maximum harmonic number is 23, which corresponds to the wavelength of 36 nm. This is in good agreement with the experimental findings of [13], where harmonics down to 45 nm were observed. Note that both the geometry of the bowtie antenna and the input intensity are not exactly defined in [13] which can lead to deviations between theory and the experiment. In contrast to the nanocone, in the case of the bowtie antenna a relatively low field enhancement due to larger curvature radii leads to a smaller amplitude of electron motion which, together with a relatively homogeneous field distribution, makes the model modifications less important than in the case of the considered nanocone. Our calculations predict that the cutoff value has increased by only roughly 20% due to the effects of the inhomogeneity and the metallic surface.

-
- [1] M. Hentschel, R. Kienberger, C. Spielmann, G. A. Reider, N. Milosevic, T. Brabec, P. Corkum, U. Heinzmann, M. Drescher, and F. Krausz, *Nature* **414**, 509 (2001).
 - [2] A. Paul *et al.*, *Nature* **421**, 51 (2003).
 - [3] X. Zhang *et al.*, *Nat. Phys.* **3**, 230 (2007).
 - [4] P. B. Corkum and F. Krausz, *Nat. Phys.* **3**, 381 (2007).
 - [5] H. Kapteyn, O. Cohen, I. Christov, and M. Murnane, *Science* **317**, 775 (2007).
 - [6] M. F. Kling and M. J. J. Vrakking, *Annu. Rev. Phys. Chem.* **59**, 463 (2008).
 - [7] F. Krausz and M. Ivanov, *Rev. Mod. Phys.* **81**, 163 (2009).
 - [8] G. Sansone *et al.*, *Nature* **465**, 763 (2010).
 - [9] S. A. Maier, "Plasmonics: Fundamentals and applications", Springer, Berlin 2007.
 - [10] M. Pelton, J. Aizpurua, G. Bryant, *Laser Photon. Rev.* **2**, 136 (2008).
 - [11] S. Nie and S. R. Emory, *Science* **275**, 1102 (1997).
 - [12] E. Prodan *et al.*, *Science* **302**, 419 (2003).
 - [13] S. Kim *et al.*, *Nature* **453**, 757 (2008).
 - [14] M. Lewenstein *et al.*, *Phys. Rev. A* **49**, 2117 (1994).
 - [15] Supplementary material is available for this paper at <http://prl.aps.org/>.

* Electronic address: gusakov@mbi-berlin.de